Acid and base catalyzed reaction mechanisms in bio butadiene production from 2,3-butanediol

Beruk A. Bekele[1], Jeroen Poissonnier[1], Joris W. Thybaut[1*]

[1]Laboratory for Chemical Technology, Ghent University, Technologiepark 125, B-9052, Ghent, Belgium

* Corresponding author email address: Joris.Thybaut@UGent.be.

Key words: Berty reactor, intrinsic kinetics, experimental assessment, base-dominated active sites, apparent activation energy.

Abstract

2,3-butanediol (2,3-BDO) dehydration to 1,3-butadiene (BD) is assessed over a Sc_2O_3 catalyst calcined at 800°C (Sc_2O_3_800) and compared with performance of an in-house prepared ZrO_2 (ZrO_2_HT_800) catalyst via active sites, activity, product distribution and apparent activation energies to elucidate the reaction mechanism. Sc_2O_3_800 achieved 40% (mol mol^{-1}) selectivity towards BD at complete 2,3-BDO conversion. This is due to its medium strength basic sites and weak acid sites, favoring a base-dominated mechanism and producing 3-buten-2-ol (3B2OL) as the primary product, suggesting an *E1cb-like* mechanism. Conversely, ZrO_2_HT_800 favors methyl ethyl ketone (MEK) formation due to relatively similar amounts and strength of acid and base sites, suggesting competing E1 and E2 mechanisms. Apparent activation energies for 3B2OL formation amount to 63 kJ mol^{-1} over the Sc_2O_3_800 catalyst and 38 kJ mol^{-1} over the ZrO_2_HT_800 catalyst, while MEK formation has an apparent activation energy of 64 kJ mol^{-1} over Sc_2O_3_800 and 80 kJ mol^{-1} over ZrO_2_HT_800 catalysts. The optimal process conditions for bio-butadiene production in a single step over Sc_2O_3_800 are a temperature of 385°C, inlet 2,3-BDO partial pressure of 0.2 bar and a space time amounting to 1130 kg s mol^{-1}.

1. Introduction

The widespread utilization of fossil feedstocks, e.g. petroleum, has significantly contributed to the growth of the global chemical industry over the last century, serving as the primary source for manufacturing a broad spectrum of chemicals [1]. Despite its contribution to the chemical industry's growth and advancement of human welfare, fossil feedstocks utilization has resulted in significant environmental consequences, primarily through the emission of greenhouse gases (GHG) that contribute to floods, droughts, and tropical storms. These consequences have become too substantial to overlook, and the continued reliance on fossil feedstocks may jeopardize the sustainability of humankind's civilization in the near future [2].

Our present-day society must prioritize the reduction of its dependency on fossil feedstocks and, as an alternative, explore sustainable feedstocks and environmentally friendly production methods [3,4]. A potential solution to achieve this objective is by implementing the principles of green chemistry, which aim at reducing or eliminating the use or generation of hazardous substances while promoting sustainability [2, 3, 5]. To achieve this, substituting fossil feedstocks with biomass derived ones would be a good first step. This transition to biomass-based feedstocks is paramount since it reduces greenhouse gas emissions and contributes to resource conservation and carbon neutrality [3].

The production of 1,3-butadiene (BD) is vital in the current scenario where the primary commercial production method, naphtha steam cracking, is associated with vast CO_2 emissions (1.5 ton ton^{-1} ethylene)[6]. In addition, the recent feedstock shift towards shale gas resulted in a substantially decreased BD yield [6–8]. This presents an opportunity to develop a more sustainable, biobased and on-purpose approach to produce BD, thereby ensuring lower CO_2 emissions and energy requirements, ultimately allowing an environmentally friendly alternative process. Within this context, several feedstocks including ethanol, butanol and butanediols (BDO) have emerged as promising bio-based feedstock for BD production [9–14]. BDOs are interesting due to their new biobased production and 4-carbon nature allowing for a good atom economy. Several reports indicate their production from various biomass substrates such as wheat straw, glucose, xylose, sucrose, etc. [15–19]. 2,3-butanediol (2,3-BDO) production from glucose has made significant progress and is currently considered a potential feedstock for BD production. Yields amounting to 50% (wt) have been reported so far [17].

The catalytic dehydration of 1,3-BDO and 1,4-BDO have also been investigated as an alternative feedstock to 2,3-BDO for BD production. The catalysts used for 1,3-BDO are SiO_2-Al_2O_3, HZSM-5, CeO_2/Mordenite and Al/SBA-15, where SiO_2-Al_2O_3 resulted in lower performance at a yield of 27%, with the others yielding between 45% and 60% [17]. In the case of 1,4-BDO, the catalysts used are SiO_2-Al_2O_3, CeO_2 and Yb_2O_3 where Si_2O_3-Al_2O_3 resulted in around 18% yield towards BD and CeO_2 in around 66% yield [17, 20]. A single work reported on the uncommon Yb_2O_3 material, leading to an exceptionally high yield amounting to 97% [21]. Apart from the yields that can be achieved, it must be noted that 1,4-BDO as a biobased diol is less relevant for BD production given its large-scale conventional production in the nylon industry.

The dehydration of 2,3-BDO towards BD has been challenging from a selectivity perspective using common acid catalysts such as zeolites and alumina [22–28]. This challenge originates from the thermodynamically favored side product, methyl ethyl ketone (MEK), which can form on different types of acid sites as they occur in various catalysts [6]. While acid-containing catalysts are most frequently employed for dehydration reactions, they are not the sole option, however. Catalysts with predominantly basic sites are also active and selective towards specified products [29].

Solid base catalysts have many applications, such as aldol condensation, double bond isomerization, dehydration, and dehydrogenation [29]. Alkaline earth oxides from solid base catalysts are the most investigated ones because of their activity in proton abstraction [30]. MgO is the most widely used base catalyst in reactions such as aldol condensation and double bond isomerization. Rare earth oxides are another group of catalysts exhibiting basic properties [31]. Rare earth oxides contain weak basic sites and are selective to the Hoffmann elimination product in the dehydration of 2-butanol (2BOL) and generally allow α-olefin formation [32].

Basic catalysts allow a reaction to proceed through a different path, resulting in a different product distribution compared to acid catalysts. The product distribution of 1-butene isomerization is highly sensitive to the nature of the catalyst, and the initial *cis-to-trans* ratio has been employed as a test reaction for determining the acid and base characteristics of catalysts [33]. In the case of acid catalysts, it results in an initial *cis-to-trans* ratio of 1. In contrast, basic catalysts result in a higher *cis*-to-*trans* ratio, typically ranging from 2 to 5, at the beginning of the reaction [34].

In the case of (bio-)alcohol feedstocks, solid acid catalysts form olefins and ethers as products, while base catalysts result in aldehydes and ketones [29]. The difference in the product spectra is due to differences in the reaction network/mechanism when acid and base catalysts are employed as catalysts, resulting in different product distributions. E.g. the dehydration of 2-butanol results in 1-butene over rare earth oxides while it results in 2-butene over acidic catalysts [29]. Another example is the dehydration of 5-amino-1-pentanol over basic rare earth oxides such as Tm_2O_3, Yb_2O_3 and Lu_2O_3, resulting in the formation of 4-penten-1-amine at 425°C while over acidic non-rare earth oxides such as Al_2O_3, SiO_2, TiO_2 cyclic amines such as piperidine are formed as a major product at temperatures exceeding 300°C [31].

In the case of 2,3-BDO dehydration, Sc_2O_3 is reported in the literature for its selective formation of 3B2OL [35]. Duan et al. reported 3B2OL selectivity reaching as high as 85% (mol mol^{-1}) at 99% (mol mol^{-1}) 2,3-BDO conversion during dehydration at 325°C over Sc_2O_3 calcined at 800°C [35]. Nakazano et al. further investigated specific synthesis methodologies and calcination temperatures for Sc_2O_3 catalysts. Their work demonstrated hydrothermal aging as the preferred synthesis method for employing Sc_2O_3 in 2,3-BDO dehydration towards BD. Their catalyst calcined at 800°C, exhibits a BD yield exceeding 80% (mol mol^{-1}) at 411°C [36, 37]. Duan et al. and Zeng et al. investigated a dual bed catalytic system for converting 2,3-BDO to BD. In this system, Sc_2O_3 was used as the first catalyst in the bed in both cases, as it exhibited high selectivity (>85% mol mol^{-1}) towards the production of 3B2OL. Subsequently, in the second bed, 3B2OL was dehydrated to BD using Al_2O_3 or other catalysts that were found to be effective for this step [36,38]. The result was the formation of BD with a selectivity amounting to 94% (mol mol^{-1}) at complete 2,3-BDO conversion at 318°C only. This means that this configuration of the catalyst bed allowed complete 2,3-BDO dehydration at a lower temperature than for Sc_2O_3 as sole catalyst, which

required at least a temperature of 411°C to obtain a yield of 88% (mol mol^{-1}). However, Zeng et al. found a maximum selectivity towards BD amounting to 60% (mol mol^{-1}) at complete 2,3-BDO conversion and 375°C with the same dual bed (Sc_2O_3+Al_2O_3). They obtained a yield of 28% (mol mol^{-1}) of MEK, while virtually no MEK was reported in the case of Duan et al. [38]. In addition, Zeng et al. also observed that the selectivity towards BD decreased with increasing temperature to 400°C [38].

In this work, an experimental, kinetic and mechanistic study of 2,3-BDO dehydration over a Sc_2O_3 catalyst is performed, aiming at elucidating the reaction mechanism over Sc_2O_3 and comparing it with the one over a previously investigated ZrO_2 catalyst. To achieve this goal, catalyst characterization is used to probe the available active sites and kinetics testing to determine the effect of operating conditions on 2,3-BDO conversion and product distribution.

2. Procedures

2.1 Materials and catalyst

Scandium(III) oxide (99.9% trace rare metal basis) was obtained from Sigma-Aldrich. The obtained catalyst was calcined at 800°C and denoted as Sc_2O_3_800. As described in our previous work, ZrO_2 was synthesized via a hydrothermal methodology and denoted as ZrO_2_HT_800 [39]. Comprehensive characterization of Sc_2O_3_800, including N_2 isotherms, NH_3 and CO_2-TPD profiles and CO_2-TPD-DRIFT profiles are described in the next section. However, only the methodology for measuring ZrO_2_HT_800 sample is presented here; the remaining ones can found in our previous work [39].

2.2 Catalyst characterization

2.2.1 Surface area and porosity measurement

The catalyst surface area was investigated by N_2 adsorption in a Micromeritics Tristar II apparatus. Prior to the measurement, the catalyst was degassed at 573 K for 3 h to eliminate any remaining species from the surface. The specific surface area was determined using the Brunauer-Emmett-Teller (BET) method with p/p^o ranging from 0.01 to 0.99 [40]. The Barrett-Joyner-Halenda (BJH) method was employed to determine the average pore size, total pore volume and pore size distribution from the desorption isotherm [40].

2.2.2 Acidity and basicity measurement

To assess the acidity and basicity of the employed sample, Temperature Programmed Desorption (TPD) was performed using NH_3 and CO_2 as probe molecules, respectively. An AutoChem II 2920 (Micromeritics) instrument equipped with a Thermal Conductivity Detector (TCD) has been employed for this purpose. For acidity measurements, the sample (± 0.2 g) was first treated with high purity (99.999 %) He at a flow rate of 25 ml min^{-1} during heating to 600°C, kept at the same temperature for 1 h and then cooled to 150°C. The sample was then saturated with a flow containing 4% (mol mol^{-1}) NH_3 balanced in He at 150°C for 30 min. Physisorbed NH_3 was removed by flushing with pure He at 150°C for 1 h. The TPD was performed by increasing the temperature to 600°C at a heating rate of 10°C min^{-1}. The amount of ammonia desorbed is correlated to the peak area under the NH_3-TPD curve and quantified using a calibration curve for NH_3.

To determine the basicity of the catalyst, CO_2-TPD measurements were performed. The sample (± 0.2 g) was pretreated in the same manner as for acidity measurement. The sample was saturated with a flow containing pure CO_2 at 120°C for 4 h. Physisorbed CO_2 was removed by flushing with pure He at 120°C for 1 h. The analysis was carried out by increasing the temperature to 600°C at a

heating rate of 10°C min^{-1}. The amount of CO_2 desorbed is correlated to the area under the CO_2-TPD curve and quantified using a calibration curve for CO_2.

2.2.3 CO_2-TPD-FTIR measurements

CO_2-TPD-FTIR measurements were performed using a Bruker Tensor 27 spectrometer equipped with a liquid N_2 cooled MIR source and KBr optics, running under OPUS software. The reaction system consists of a Harrick plug flow reactor inside a Praying Mantis equipped with ZnSe windows. Absorption mode was used. 15 mg of each sample was mixed with 110 mg of KBr and placed in the sample bed. First, the sample was pretreated by increasing the temperature under He flow to 325°C and holding it for 70 min. The temperature was subsequently decreased to 120°C, and background measurements were taken. Next, 10% CO_2 balanced in He was used to perform the adsorption of CO_2 on the treated sample for 30 min and the spectra were recorded. Then, temperature programmed desorption was carried out in He to 325°C, and 400°C by increasing the temperature at 5°C min^{-1} and recording the FTIR spectra at 120°C. In addition, the effect of dosing CO_2 at 2.5%, 5%, and 10% was determined with the respective amounts and the spectra recorded at 120°C.

2.3 Definitions and data analysis

The data analysis followed the same procedure as in our previous work, where the peak areas of each component were measured using GC-FID with CH_4 as internal standard [39]. The carbon balance was verified to be closed, with a maximum deviation of 5% for the Sc_2O_3_800 dataset. Finally, outlet flow rates for each component were determined and the conversion of 2,3-BDO (X_{BDO}) and selectivity (S_i) towards each product i were calculated via Equations 1 and 2 [39].

$$X_{BDO} = \frac{F^0_{BDO} - F_{BDO}}{F^0_{BDO}} \cdot 100\% \qquad [\text{mol mol}^{-1}] \qquad (1)$$

$$S_i = \frac{a_{Ci} \cdot F_i}{4 \cdot (F_{BDO}^0 - F_{BDO})} \cdot 100\% \qquad [\text{mol mol}^{-1}] \qquad (2)$$

Where a_{Ci} represents the carbon number of component *i*, F_i, its molar flow rate in the reactor effluent and F_{BDO}^0 the 2,3-BDO molar inlet flow rate. The factor four stems from the carbon number of 2,3-BDO [39].

2.4 Intrinsic kinetics measurements

Intrinsic kinetic experiments were conducted in a Berty gas-solid Continuous Stirred Tank Reactor (CSTR) with complete internal mixing [41]. Comprehensive information about the reactor can be found in our previous work [42]. The range of operating conditions is listed in Table 1, which are situated in the intrinsic kinetic regime as verified via the relevant correlations, see Table 2.

Table 1 Summary of experimental operating conditions for 2,3-BDO dehydration over Sc_2O_3.

Operating condition	Range
W_{cat} (g)	1-2
T (°C)	325 – 400
p_{tot} (bar)	10
$p_{2,3-BDO}$ (bar)	0.04 - 0.9
$\frac{W}{F}$ (kg s mol^{-1})	90 - 1130

To avoid potential heat and mass transfer limitations during the kinetics measurements, the criteria are applied at the most severe operating conditions. The Carberry number was used to determine the absence of external mass transfer limitations, which is listed in Table 2 [43]. The highest calculated Carberry number amounted to 10^{-10}, which is significantly below the limiting value of 0.05. Internal mass transfer limitations were assessed via the Weisz-Prater criterion. The highest

value of Weisz modulus, amounting to 10^{-10} for 2,3-BDO, is well below the limiting value of 0.08 [44].

The absence of external and internal heat transfer limitations was assessed via the Mears and Anderson criteria, as shown in Table 3. The interphase (external) and intraparticle (internal) heat transport temperature rise amounts to 10^{-8} K and 10^{-13} K, respectively, which are well below the limiting value of 2.7 K [45].

Table 2 Intrinsic kinetic measurement verification at operating condition [325℃].

Phenomenon	Criterion	Calculated value compared to criterion
External mass transport	$\text{Ca} = \frac{\left(R_{v,i}^{obs}\right)}{k_g\, a_v\, c_{i,b}} = \frac{c_{i,b} - c_{i,s}}{c_{i,b}} < \frac{0.05}{n}$	$10^{-10} < 0.05$
Internal mass transport	$\Phi = \left(\frac{n+1}{2}\right) \frac{R_{v,i}^{obs}\left(\frac{d_p}{6}\right)^2}{\mathcal{D}_{i,eff} c_{i,S}} < 0.08$	$10^{-10} < 0.08$
External (interphase) heat transport	$\frac{E_j R_{v,i}^{obs} [\Delta H_r] \rho\, d_p}{2\, R\, h\, T_o^2} < 0.15$	$10^{-8} < 0.15$
Internal (intraparticle) heat transport	$\frac{E_j R_{v,i}^{obs} [\Delta H_r]\, d_p}{4\, R\, \lambda\, T_o^2} < 0.75$	$10^{-13} < 0.75$

3. Characterization results

3.1 Surface area and N_2 sorption isotherm

The surface area, pore volume, pore size and adsorption isotherm of Sc_2O_3_800 and ZrO_2_HT_800 catalysts are compared via N_2 physical adsorption. The XRD pattern for ZrO_2_HT_800 is available in our previous manuscript [39]. The average diameter of the accessible pores are similar; 16.1 nm for ZrO_2_HT_800 and 14.7 nm for Sc_2O_3_800. However, the pore volume of Sc_2O_3_800 (0.08 cm^3/g) is smaller than that of ZrO_2_HT_800 (0.2 cm^3/g), see Table 3. The adsorption-desorption

isotherms of these materials are depicted in Figure 1. According to the IUPAC classification of N_2 isotherms, Sc_2O_3_800 exhibit type IV isotherms, characterized by a H3 hysteresis loop, which is indicative of a mesoporous material with non-rigid aggregates of *plate-like* particles while ZrO_2_HT_800 exhibited type V isotherm with H2 hysteresis loop representing a narrow range of uniform mesopores [39, 40]. In addition, the distribution of pore volume as a function of the pore width for both catalysts can be found in the Supporting Information S1.

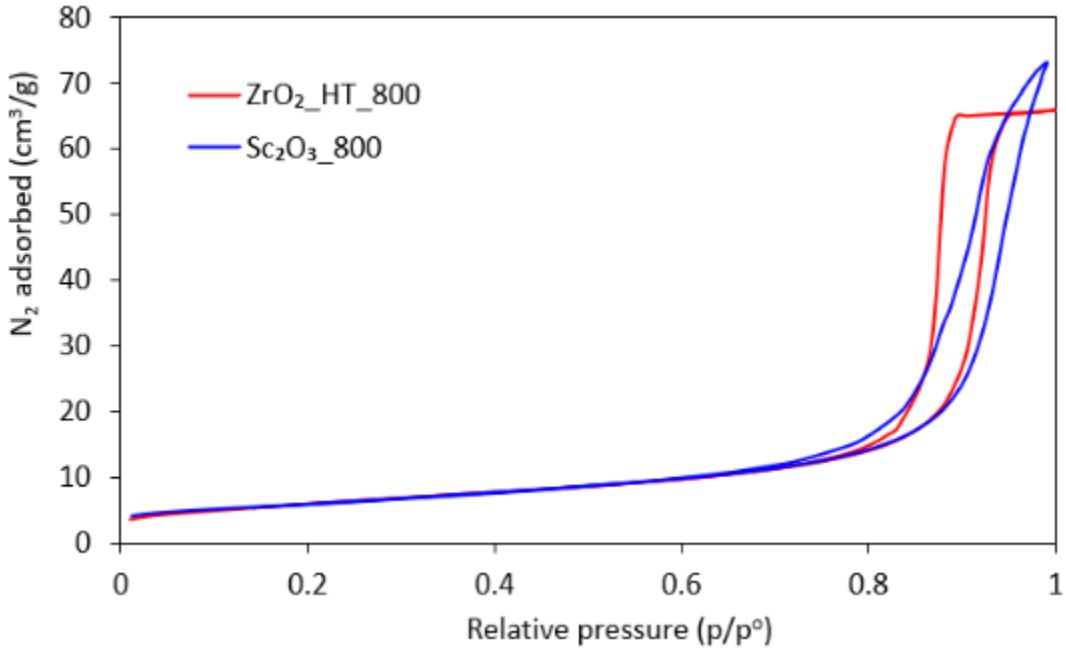

Figure 1: N_2 adsorption-desorption isotherms for Sc_2O_3_800 and ZrO_2_HT_800.

3.2 Acidity and basicity

The acidity and basicity of Sc_2O_3_800 and ZrO_2_HT_800 were compared. The Sc_2O_3_800 exhibited lower acidity, i.e. 0.09 mmol g^{-1} but much higher basicity i.e. 0.7 mmol g^{-1} compared to ZrO_2_HT_800, containing 0.2 and 0.13 mmol g^{-1} acidic and basic sites, respectively, see Table 3. The strength of the sites is determined from the normalized NH_3 or CO_2 uptake as a function of temperature, see Figure 2 and Table 3. The strength and amount of acidity in Sc_2O_3_800 are lower

than ZrO_2_HT_800 however in terms of basicity, the Sc_2O_3_800 contains much more basic sites which are specifically stronger than the ones in ZrO_2_HT_800. The strength of the sites is inferred from the desorption temperatures that indicate that ZrO_2_HT_800 contains stronger acid sites than Sc_2O_3_800. In terms of basicity, ZrO_2_HT_800 has weak sites (<200°C) and Sc_2O_3_800 has medium strength sites (420°C).

Table 3 Specific surface area, pore volume, average pore size, acidity and basicity of ZrO_2_HT_800 and Sc_2O_3_800

Catalyst	**BET surface area (m^2 g^{-1})**	**BET average pore diameter (nm)**	**Pore volume at p/p°=0.95**	**NH_3 uptake (mmol g^{-1})**	**CO_2 uptake (mmol g^{-1})**
ZrO_2_HT_800	38	16.1	0.2	0.2	0.13
Sc_2O_3_800	21.4	14.7	0.08	0.09	0.7

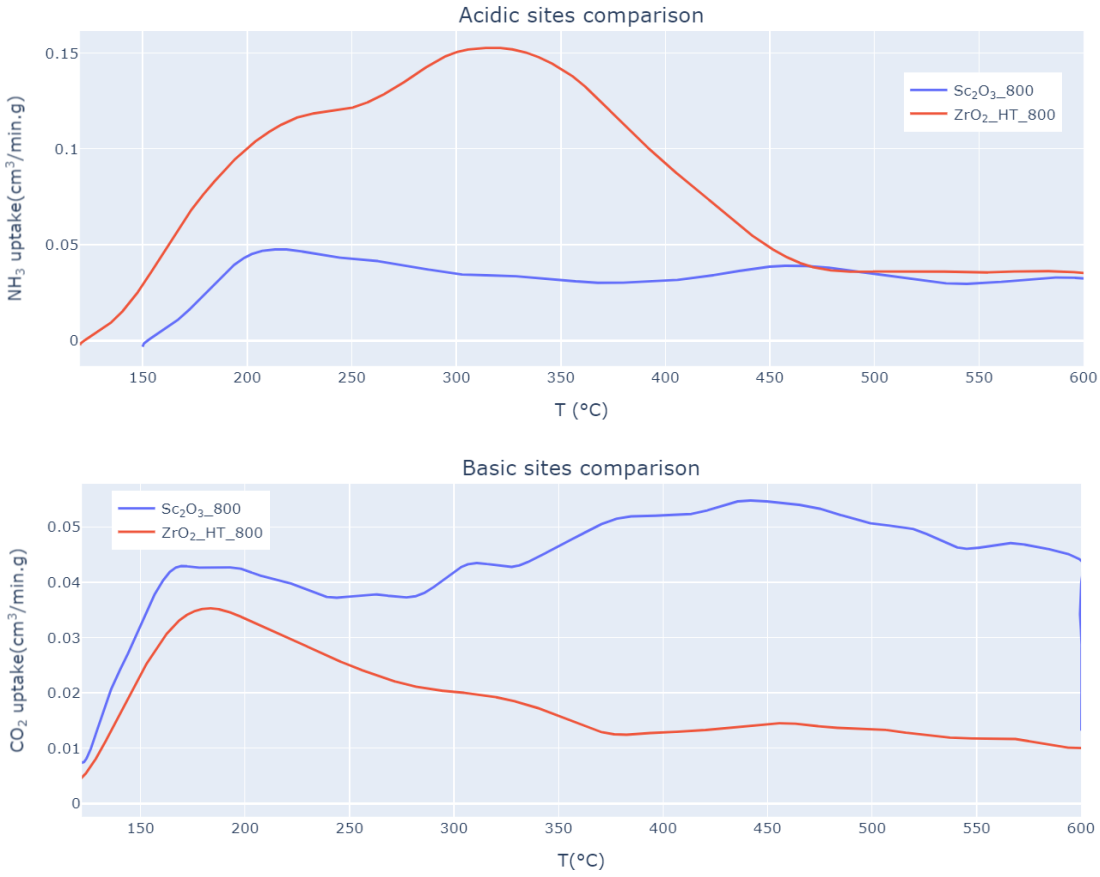

Figure 2: NH_3-TPD (top) and CO_2-TPD (bottom) for ZrO_2_HT_800 and Sc_2O_3_800 catalyst samples.

3.3 CO_2-TPD FTIR Results

Given the abundance of basic sites in both ZrO_2_HT_800 and Sc_2O_3_800 and their relevance for the desired reaction, their further investigation is considered crucial. The CO_2-TPD-FTIR measurement is important for comparison of the basic adsorption sites in the metal oxides, determining the available species on the surface and in determining stability of the species at typical reaction temperatures, c.a., 325 and 400°C. The spectra for Sc_2O_3_800 catalyst in Figure 3 at both temperatures display peaks in the range of 1340-1656 cm^{-1}. The major peaks found in both catalysts in the range 1300-1330 cm^{-1} and 1600-1630 cm^{-1} correspond to bidentate carbonate species. On one hand, a peak that is distinct for Sc_2O_3_800 centered at 1410 cm^{-1}, is attributed to polydentate carbonate species. On the other hand, peaks distinct for ZrO_2_HT_800 are at 1510-1530 cm^{-1}, 1363 cm^{-1} and 1562 cm^{-1} where the first two are attributed to monodentate carbonate species while the last one is attributed to a hydrogen carbonate species. Thus, the CO_2-TPD FTIR analysis revealed peaks for hydrogen carbonate species only in the case of ZrO_2_HT_800 indicating the presence of Bronsted sites. While polydentate species are observed only in the case of Sc_2O_3_800, characterized by Lewis base sites with high stability and lower reactivity. The stability of the species at higher temperatures during desorption at the nominal and maximal operating temperatures of the reaction conditions can be found in the Supporting Information, Figure S2. The other peaks at a wavenumber around 3600-3800 cm^{-1} are attributed to adsorbed water species, which desorb by increasing the temperature to 325°C (not shown) [46]. These findings suggest that Sc^{3+} and O^{2-} species are most probably the predominant active sites present in Sc_2O_3_800 in the temperature range of 325°C to 400°C and are responsible for the catalytic activity.

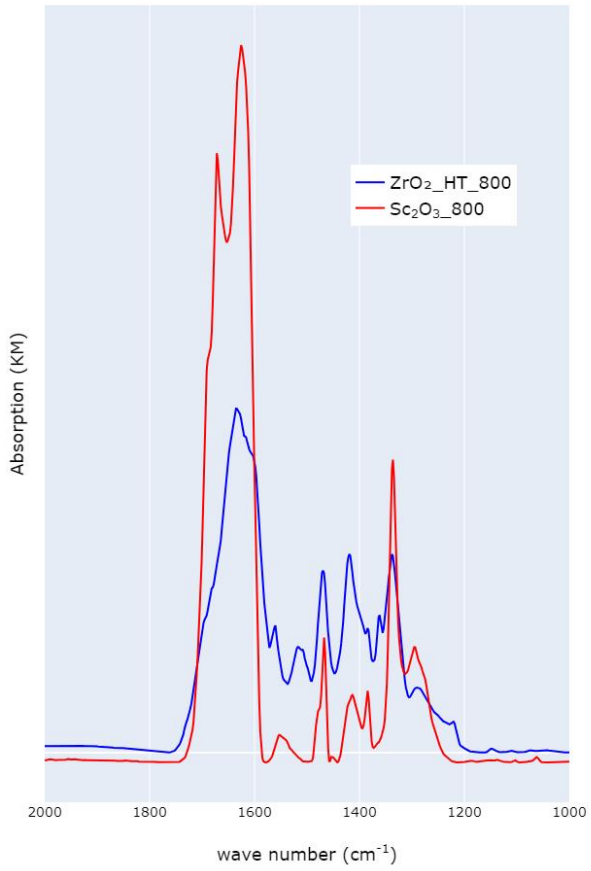

Figure 3: Evolution of Infrared spectra for surface species of , Sc_2O_3_800 up on CO_2 adsorption. The spectra from 2200 to 3700 cm^{-1} have been removed for clarity.

4. Kinetics measurement results

The dehydration of 2,3-BDO proceeds through four main routes, from which three are effectively denoted as ‘dehydration’ and one as ‘dehydrogenation’, see Figure 4. The dehydration routes yield 3B2OL, MEK, and 2-methyl propanal (2MPAL). Further dehydration of 3B2OL yields BD, while hydrogenation of MEK and 2MPAL leads to 2BOL and *iso*-butanol (iBOL) respectively which could further dehydrate towards their respective butene. The dehydrogenation pathway forms 3-hydroxy-2-butanone (3H2B), which can either dehydrogenate further to 2,3-butadione (not

shown) or condense to dimethyl phenols (DMP). These pathways are detailed in our previous manuscript [39].

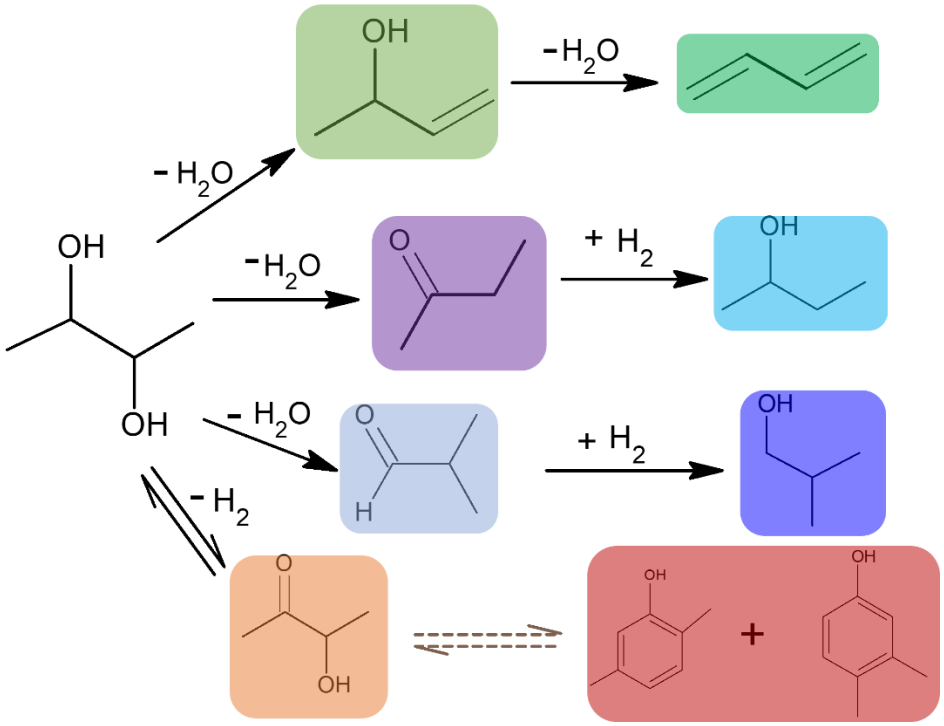

Figure 4: proposed reaction network for 2,3-BDO dehydration over Sc_2O_3_800.

4.1 Space time effect

The space time effect during 2,3-BDO dehydration is investigated at 325°C and 375°C and an inlet 2,3-BDO partial pressure of 0.46 bar, see Figure 5. The 2,3-BDO conversion increases from 8% (mol mol^{-1}) to 16% (mol mol^{-1}) at 325°C with increasing space-time from 90 kg s mol^{-1} to 226 kg s mol^{-1}. Although the catalyst activity at 325°C is minimal, the conversion of 2,3-BDO does increase with the space time. At 375°C, the 2,3-BDO conversion increased from 56% (mol mol^{-1}) at 90 kg s mol^{-1} to 82% (mol mol^{-1}) at 226 kg s mol^{-1}, highlighting the effect of space time, especially at higher temperatures.

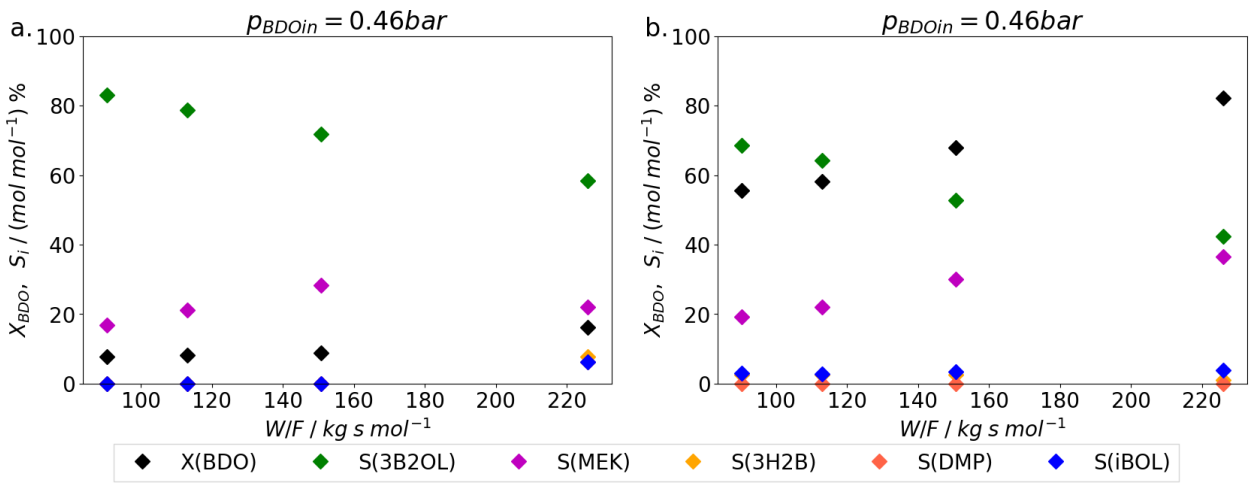

Figure 5: Effect of space-time on 2,3-BDO conversion and product distribution during 2,3-BDO dehydration over Sc_2O_3_800 at inlet 2,3-BDO inlet partial pressure of 0.46 bar and a. 325°C and b. 375°C.

The product distribution at a 2,3-BDO conversion of 8% (mol mol^{-1}), obtained at 325°C, indicates the presence of only 3B2OL and MEK at approximately 80% and 20% (mol mol^{-1}), respectively which points to the primary product nature of 3B2OL and MEK. At 2,3-BDO conversion amounting to 60% (mol mol^{-1}), obtained at 375°C and 90 kg s mol^{-1}, the product distribution shifted towards a lower 3B2OL selectivity of 68% (mol mol^{-1}) and, correspondingly to the formation of minor products such as 3H2B, iBOL and 2BOL each amounting to 3% (mol mol^{-1}). With increasing 2,3-BDO conversion, a higher selectivity towards MEK is observed, especially at 375°C. Higher order products such as iBOL and DMP are also formed at the higher conversion, albeit to a limited extent. The trend of the 2,3-BDO conversion in combination with the product distribution confirms that these are secondary products. The highest joint selectivity obtained towards MEK and 2BOL amounts to 38% (mol mol^{-1}) while that towards 2MPAL and iBOL amounts to 10% (mol mol^{-1}).

The product distribution at more extreme temperatures of 385°C and 400°C, and 2,3-BDO conversion (exceeding 85% (mol mol^{-1})), is shown in Figure 6. The selectivity towards 3B2OL decreased from 68% (mol mol^{-1}) at 150 kg s mol^{-1} to only 10% (mol mol^{-1}) at 1130 kg s mol^{-1} with

a corresponding increase in selectivity towards MEK from 5% (mol mol^{-1}) to 35% (mol mol^{-1}) and BD from 0% (mol mol^{-1}) to 40% (mol mol^{-1}) during the 2,3-BDO dehydration at 385°C and inlet 2,3-BDO partial pressure of 0.2 bar. A maximal selectivity towards DMP was observed at 226 kg s mol^{-1} amounting to 12% (mol mol^{-1}) which suggests formation via direct condensation of formed 3H2B due to the high temperature. As the space time increases, there is also a slight increase in selectivity towards 2BOL and iBOL, reaching 3.2% and 5.5% (mol mol^{-1}), respectively. A rise in space time induces the second dehydration towards BD especially at temperatures as high as 385°C and 400°C including formation of some undesired products. The joint selectivity towards 3B2OL and BD actually decreases from 70% (mol mol^{-1}) to 49% (mol mol^{-1}) at 385°C while that of MEK and 2BOL increases from 12% (mol mol^{-1}) to 36% (mol mol^{-1}).

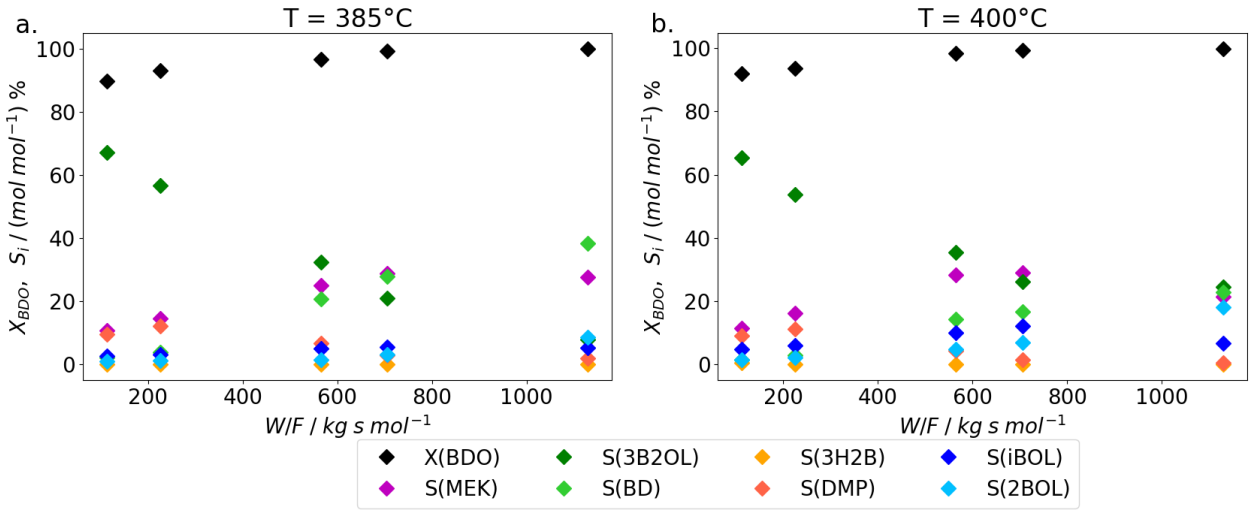

Figure 6: Effect of space-time on 2,3-BDO conversion and product distribution during 2,3-BDO dehydration over Sc_2O_3_800 at an inlet 2,3-BDO partial pressure of 0.2 bar at a. 385°C and b. 400°C.

The 2,3-BDO conversion at 400°C exceeds 90% (mol mol^{-1}) at all space times as shown in Figure 6 b. The selectivity towards 3B2OL amounts to 65% (mol mol^{-1}) at 113 kg s mol^{-1} and decreases to 24% (mol mol^{-1}) at 1130 kg s mol^{-1}. Correspondingly, the selectivity towards MEK increases from 11% (mol mol^{-1}) at 113 kg s mol^{-1} to a maximum of 35% (mol mol^{-1}) at 565 kg s mol^{-1} and decreases back to 21% (mol mol^{-1}) at 1130 kg s mol^{-1}. The selectivity towards BD increased from

2% (mol mol^{-1}) at 113 kg s mol^{-1} to 23% (mol mol^{-1}) at 1130 kg s mol^{-1}. The maximal selectivity towards DMP observed amounts to 11% (mol mol^{-1}) at 226 kg s mol^{-1} and decreases with space-time reaching 0.6% (mol mol^{-1}) at 1130 kg s mol^{-1}. No significant amounts of 3H2B are observed at most of the space times due to fast consumption in case DMP is significantly formed. Thus, the joint selectivity of DMP and 3H2B decreases from 9.6% (mol mol^{-1}) to 0.5% as the space time increases from 113 to 1130 kg s mol^{-1}. As the space time increases, there is a slight increase in selectivity towards both 2BOL and iBOL. The selectivity towards 2BOL increases from 7% (mol mol^{-1}) at 113 kg s mol^{-1} to 18% (mol mol^{-1}) at 1130 kg s mol^{-1}. On the other hand, the selectivity towards iBOL decreases from 12% (mol mol^{-1}) at 113 kg s mol^{-1} to 7% (mol mol^{-1}) at 1130 kg s mol^{-1}. Hence, at 400°C, the selectivity towards BD is limited to 23% (mol mol^{-1}) due to the competitive formation of MEK limiting the formation of 3B2OL, see Figure 6b. The joint selectivity towards 3B2OL and BD decreases from 67% (mol mol^{-1}) at 385°C to 47% (mol mol^{-1}) at 400°C due to formation of even more side products.

4.2 Temperature effect

The temperature effect on 2,3-BDO dehydration over the Sc_2O_3_800 catalyst is assessed at 150 kg s mol^{-1} and 226 kg s mol^{-1}, see Figure 7. The temperature effect is measured at a constant inlet 2,3-BDO partial pressure of 0.46 bar. A pronounced increase in the 2,3-BDO conversion is observed when increasing the temperature from 325°C to 375°C. At 226 kg s mol^{-1}, the 2,3-BDO conversion increased from 16% (mol mol^{-1}) at 325°C to 82% (mol mol^{-1}) at 375°C. An analogously pronounced increase in 2,3-BDO conversion was observed at 150 kg s mol^{-1}, i.e., from 8% at 325°C to 67% (mol mol^{-1}) at 375°C, hence, encompassing an extensive 2,3-BDO conversion range.

The product distribution during 2,3-BDO dehydration over Sc_2O_3_800 indicates that 3B2OL and MEK are the only products at low 2,3-BDO conversion (<10 % (mol mol^{-1})) achieved at low

temperature and space time; 325°C and 150 kg s mol^{-1}, confirming the primary nature of the two products. In contrast, at slightly higher space time (226 kg s mol^{-1}) secondary products such as iBOL and DMP emerge along with the primary products. The obtained product distributions indicate that lower space time and lower temperature are suitable for 3B2OL formation whereas a higher temperature allows formation of secondary products (including BD) suggesting that the choice of operating conditions is dependent on the aimed product (3B2OL or BD).

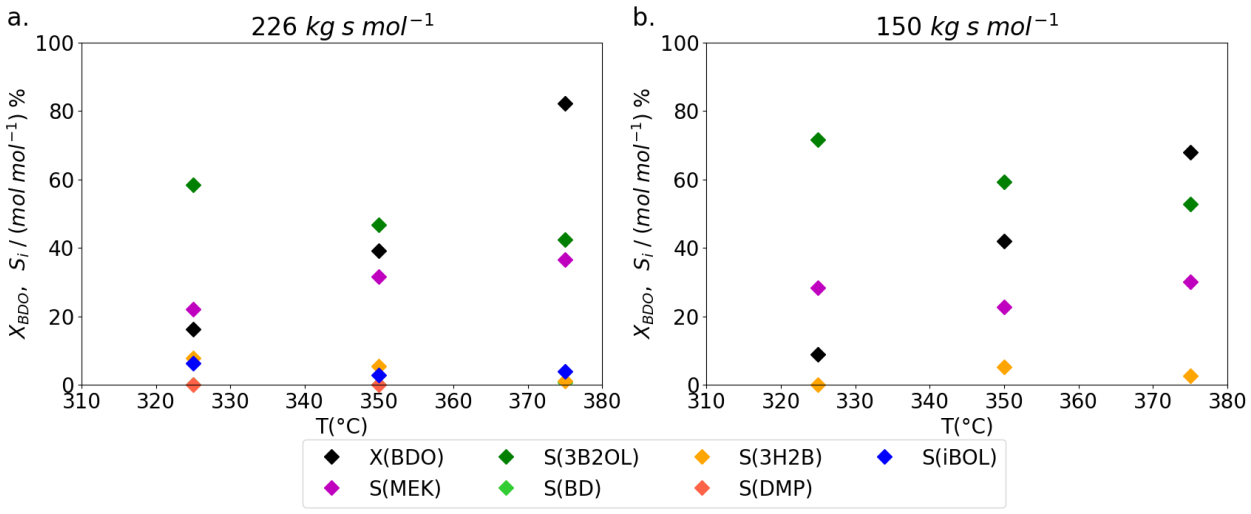

Figure 7: Effect of temperature on the 2,3-BDO conversion and product distribution during 2,3-BDO dehydration over Sc_2O_3_800 at 226 kg s mol^{-1}and 150 kg s mol^{-1} at inlet partial pressure of 2,3-BDO of 0.46 bar.

4.3 Inlet 2,3-BDO partial pressure effect

The effect of the inlet 2,3-BDO partial pressure on the 2,3-BDO conversion and product distribution is also investigated to determine optimal conditions for BD formation, see Figure 8 and Figure 9. The 2,3-BDO conversion is rather insensitive to variations in the inlet 2,3-BDO partial pressure at 325°C, as it remained constant at approximately 20% (mol mol^{-1}) in the tested inlet partial pressures range from 0.2 to 0.9 bar, see Figure 8a. At 350°C, the 2,3-BDO conversion amounts to 44% (mol mol^{-1}) at an inlet 2,3-BDO partial pressure of 0.2 bar and then slightly

increased to 50% (mol mol^{-1}) at 0.9 bar. Thus, the investigated variations in the 2,3-BDO inlet partial pressure do not significantly impact the 2,3-BDO conversion.

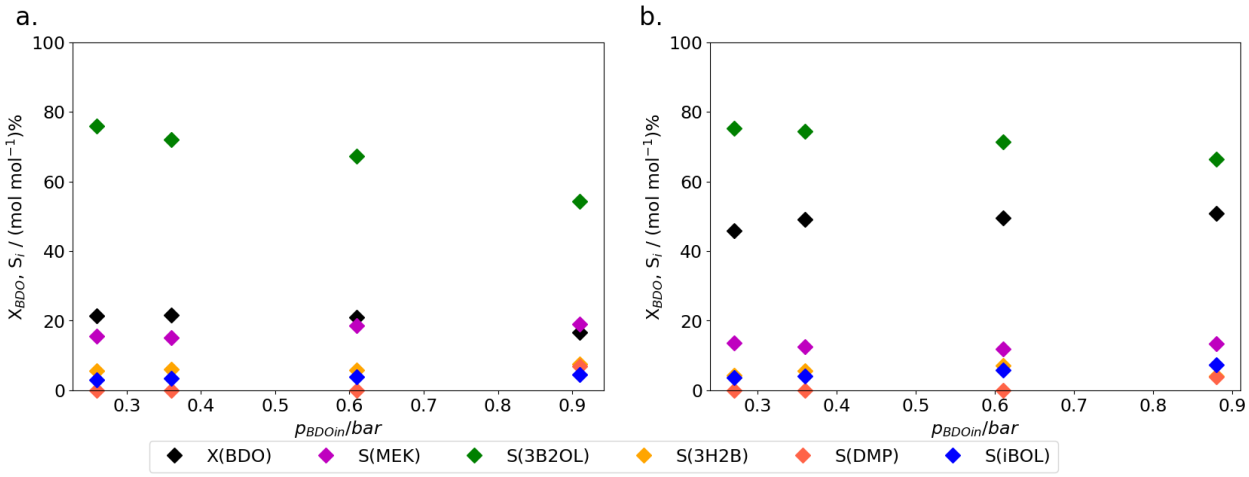

Figure 8: The effect of inlet 2,3-BDO partial pressure on the 2.3-BDO conversion and product distribution over Sc_2O_3_800 at a. 325°C and 226 kg s mol^{-1} and b. 350°C and 150 kg s mol^{-1}.

The product distributions at these two 2,3-BDO inlet partial pressures, see Figure 8a and b, are rather similar. At 325°C and 226 kg s mol^{-1}, the selectivity towards 3B2OL decreased a bit more pronouncedly from 76% (mol mol^{-1}) to 54% (mol mol^{-1}) with an increase in inlet 2,3-BDO partial pressure from 0.2 bar to 0.9 bar, while at 350°C and 150 kg s mol^{-1}, the selectivity towards 3B2OL decreased slightly from 75% (mol mol^{-1}) to 67% (mol mol^{-1}). In contrast, the selectivity towards MEK slightly increases from 15% (mol mol^{-1}) to 19% (mol mol^{-1}) due to the higher space time of 226 kg s mol^{-1} in Figure 8 a in comparison with the lower space-time of 150 kg s mol^{-1} where the selectivity towards MEK is relatively constant and limited to 14% (mol mol^{-1}).

All the products other than 3B2OL and MEK are minor ones at both conditions falling short of 7% (mol mol^{-1}) due to the low temperature in the first set of conditions and the lower space time in the second one. The partial pressure has minimal impact on the 2,3-BDO conversion thus, the experiments can be considered as a 2,3-BDO iso-conversion at 22% (mol mol^{-1}) and 44% (mol mol^{-1}), respectively. Albeit an overall limited one, the main effect of the 2,3-BDO inlet

partial pressure on the product distribution is a decrease in 3B2OL selectivity due to formation of minor side products. The joint selectivity of 2MPAL and iBOL increased from 7.8% (mol mol^{-1}) to 10.7% (mol mol^{-1}) while MEK and 2BOL increased from 22% (mol mol^{-1}) to 28% (mol mol^{-1}).

Increasing the space time at higher temperatures result in 3B2OL consumption towards BD. Hence, for BD production in a single catalyst bed, the temperature should be as high as 385°C and the space time as high as possible to allow the 2^{nd} dehydration reaction to occur while keeping the inlet 2,3-BDO partial pressure as low as possible to minimize formation of side products.

Given the promising combination of temperature and space time, the effect of the inlet 2,3-BDO partial pressure on the product distribution is also assessed at 385°C and 400°C, see Figure 9 a and b, with 2,3-BDO conversions exceeding 95% (mol mol^{-1}). At 385°C and 565 kg s mol^{-1}, the selectivity towards 3B2OL exhibits a shallow maximum amounting to 45% (mol mol^{-1}) at 0.12 bar and decreases at higher inlet 2,3-BDO partial pressure due to BD formation. This could result from approaching full 2,3-BDO conversion and thus preventing 3H2B and DMP formation. The individual selectivity towards 3B2OL and BD both reach approximately 25% (mol mol^{-1}) at 0.4 bar. The selectivity towards MEK also increased from 19% to 25% (mol mol^{-1}) with increasing inlet 2,3-BDO partial pressure from 0.1 bar to 0.4 bar . It also shows that at a 2,3-BDO inlet partial pressure amounting to 0.2 bar at 385°C, 3B2OL started to dehydrate significantly into BD while other side products are minimized. Hence, these results indicate that there is an optimum partial pressure for each temperature to maximize the formation of BD.

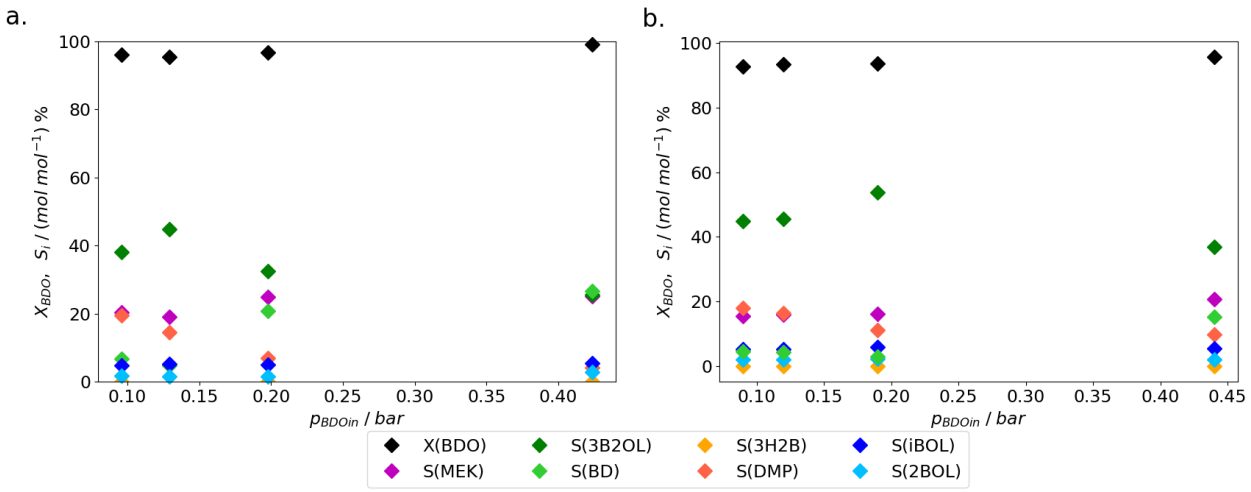

Figure 9: The effect of inlet 2,3-BDO partial pressure on the 2.3-BDO conversion and product distribution over Sc_2O_3_800 at a. 385°C and 565 kg s mol^{-1} and b. 400°C and 226 kg s mol^{-1}.

At 400°C and 226 kg s mol^{-1}, a maximum selectivity towards 3B2OL of 54% (mol mol^{-1}) is observed at an inlet 2,3-BDO partial pressure amounting to 0.2 bar. The selectivity towards 3B2OL then decreases to 36% (mol mol^{-1}) due to BD formation. The BD selectivity at this operating condition reached only 15% (mol mol^{-1}) at a 2,3-BDO inlet partial pressure of 0.4 bar. The selectivity towards BD is lower at 400°C (15% (mol mol^{-1})) than at 385°C (40% (mol mol^{-1})) due to the increased formation of other products at the higher temperature. The selectivity towards MEK also increases from 15% to 21% (mol mol^{-1}) with the inlet 2,3-BDO partial pressure from 0.1 bar to 0.4 bar, see Figure 9 b. Thus, an optimum temperature, space time and partial pressure are required to maximize the selectivity of BD during 2,3-BDO dehydration over a Sc_2O_3_800 catalyst.

4.4 Reaction network analysis

The reaction network for the dehydration of 2,3-BDO over the Sc_2O_3_800 catalyst can be determined from the intrinsic kinetic experiments over the entire 2,3-BDO conversion range. The primary products are determined from the experiments at the lowest 2,3-BDO conversions (<10% (mol mol^{-1})) at 325°C, c.q. 3B2OL and MEK are formed with selectivities amounting to

80% and 20% (mol mol^{-1}) respectively. When the 2,3-BDO conversion is increased to 50% (mol mol^{-1}), additional primary products (3H2B, 2MPAL) and secondary products (2BOL, iBOL) are also observed, see Figure 6. Although, an Meerwein-Ponndorf-Verley (MPV) reduction reaction could contribute to the interconversion of the involved components, similar as in the conversion of ethanol to BD, the secondary character of 2BOL and iBOL indicate that it does not represent a major reaction pathway in the present case [14].

As the 2,3-BDO conversion exceeds 80% (mol mol^{-1}), the selectivity towards 3B2OL decreases, due to its further conversion to BD of which the selectivity correspondingly increases. The selectivity towards 3H2B decreased due to the formation of DMP from condensation of two 3H2B molecules, eventually disappearing entirely at complete 2,3-BDO conversion. This phenomenon is attributed to the thermodynamic equilibrium between 3H2B and 2,3-BDO, as previously reported in our ZrO_2-based work [39]. The H_2 produced is primarily utilized in the further hydrogenation of 2MPAL and 2BOL products. While the potential consumption of H_2 through a reaction with lattice oxygen could be explored using H_2-TPR, however, this goes beyond the purpose of the present work. The selectivity towards MEK remained constant rather than increasing, due to an increase in selectivity towards 2BOL via hydrogenation. The reaction pathway can even become more complex via the dehydration of 2BOL to form butenes and DMPs which are susceptible to further decomposition into coke-related species. The latter represents an additional source of H_2, available for consumption in hydrogenation reactions.

Overall, a single, comprehensive reaction network allows assessing 2,3-BDO dehydration over Sc_2O_3_800 and ZrO_2_HT_800 catalysts, even if its extent over Sc_2O_3_800 is somewhat more constrained than over ZrO_2_HT_800, i.e., more side products are obtained over the latter than over the former [39]. It results in a much higher selectivity towards 3B2OL and BD in the case of

Sc_2O_3_800 catalyst. Butenes except for isobutylene are observed only in trace amounts at the highest 2,3-BDO conversion in the case of Sc_2O_3_800, while all including isobutylene up to 12% (mol mol^{-1}) were observed in the case of ZrO_2_HT_800. 2,3-butanedione from double dehydrogenation of 2,3-BDO was not observed either over Sc_2O_3_800. Hence, the reaction network of 2,3-BDO dehydration over the Sc_2O_3_800 catalyst can be summarized as shown in Figure 4.

5. Reaction mechanism

2,3-BDO dehydration involves an elimination reaction that removes water from adjacent carbon atoms, resulting in the formation of a carbon-carbon double bond. This reaction proceeds through a mechanism known as 1,2-elimination or β-elimination, which requires at least two steps: 1) proton removal or addition generating a carbocation or carbanion, respectively, 2) formation of a carbon-carbon π bond and elimination of the leaving group, c.q., water [47].

There are three types of 1,2-elimination reactions with as distinctive features the elementary steps involved and their reaction order. In an E1 mechanism, the loss of the leaving group first generates a carbocation, followed by proton removal and rearrangement of the molecule. In an E2 mechanism, the formation of the carbon-carbon double bond and removal of the leaving group occur simultaneously with proton removal from an adjacent carbon atom in a single step. In an E1cb mechanism, the abstraction of a proton from the molecule generates a carbanion, which forms a carbon-carbon double bond and eliminates the leaving group [48].

Distinguishing the exact elimination reaction mechanism for 2,3-BDO dehydration remains to be discussed. The specific catalyst employed in the reaction is a crucial factor determining the mechanism. The products generated vary depending on the catalyst employed indicative of differences in the mechanism involved, particularly in the case of a diol. Thus, Examining the

active sites that catalyze each reaction, c.q., elementary step, and the resulting product distribution is necessary to distinguish between these mechanisms.

In complex reaction networks, such as 2,3-BDO dehydration, investigating the strength of the acid and basic sites of the catalyst in conjunction with the product distribution is important to determine the mechanisms behind the reactions. E1 reactions primarily rely on acid sites, which facilitate the removal of a leaving group by protonation, generating a carbocation that can rearrange to form the product. E2 reactions, on the other hand, require a more balanced distribution of acid and base sites to effectively operate in a concerted manner. E1cb reactions rely on basic sites, facilitating the formation of anionic intermediates via deprotonation and enhancing product formation [49,50].

In the case of Sc_2O_3_800, the catalyst's basic sites are dominant; both stronger and more abundantly present, as indicated by the results in Table 3, leading to a product distribution primarily composed of 3B2OL, particularly at lower 2,3-BDO conversions, see Figure 10 b. In contrast, ZrO_2_HT_800 exhibits a more complex behavior, with more MEK formation at low 2,3-BDO conversion and competition between MEK and 3B2OL at higher 2,3-BDO conversion depending on the operating conditions, see Figure 10 a.

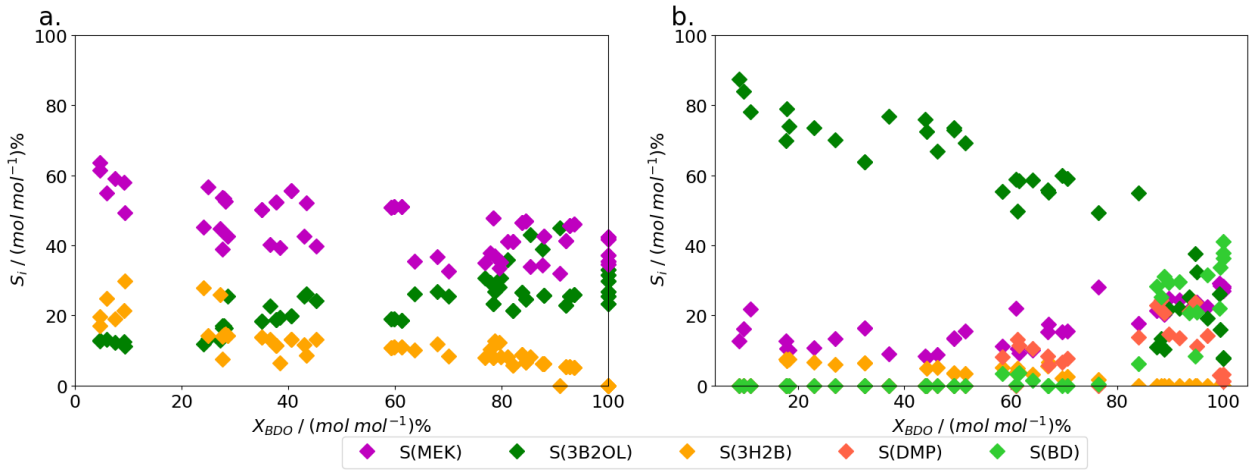

Figure 10: product distribution of a. ZrO_2_HT_800 and b. Sc_2O_3_800 catalyst during the 2,3-BDO dehydration as a function of 2,3-BDO conversion.

The predominant formation of 3B2OL during the dehydration of 2,3-BDO over a Sc_2O_3_800 catalyst at low 2,3-BDO conversion suggests that the reaction does not follow the E1 mechanism, as it would lead to (more) pronounced formation of MEK and 2MPAL via a carbocation rearrangement. Furthermore, as Sc_2O_3_800 lacks acid and basic sites with cooperative and comparable strength and number, denoted as concerted acid-base sites, thus, the E2 mechanism is unlikely over this catalyst. Therefore, considering the catalyst's base-dominated active site (See section 3.2) and the primary product spectrum, it appears that the reaction behaves as one would expect for an E1cb mechanism. This mechanism involves the initial abstraction of a proton from the β-carbon of 2,3-BDO, generating a carbanion intermediate. Subsequently, the formation of a π C-C bond and elimination of the leaving OH^- occurs, leading to the formation of 3B2OL and H_2O. In summary, the reaction proceeds stepwise through proton abstraction and intermediate formation followed by elimination, ultimately producing 3B2OL and H_2O, see Figure 11.

As investigated using CO_2-TPD DRIFT the active sites of the catalyst are able to adsorb only carbonate species, implying that the active sites could consist of oxygen vacancies and Sc cation species. It has been reported previously that the interaction of both oxygen defects and Sc cations are required to carry out the dehydration mechanism, shown in Figure 11 [37].

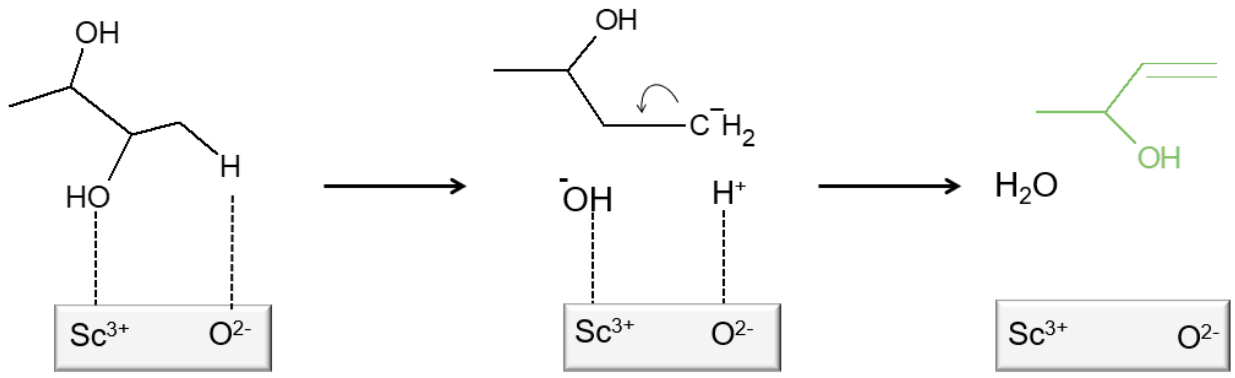

Figure 11:Proposed mechanism of 3B2OL formation over Sc_2O_3 [37].

In the case of ZrO_2_HT_800, the catalyst has acid-base concerted sites, which have been described in our previous work [39]. The more complex product distribution observed indicates a competition between E2 and E1 mechanisms, depending on the operating conditions and 2,3-BDO conversion. The active sites that can form concerted acid-base sites lead to the formation of 3B2OL via the E2 mechanism, while unpaired acid sites available on the surface result in the formation of MEK and 2MPAL via the E1 mechanism. The proposed mechanism for the formation of 3B2OL and MEK over ZrO_2_HT_800 is illustrated in our previous work [39].

Kinetic analysis of the data obtained in both cases can be used to further support this hypothesis. The evolution of the 2,3-BDO conversion as a function of temperature over Sc_2O_3_800 indicates that the overall reaction rate is much slower than over ZrO_2_HT_800. Moreover, comparison of the turnover frequency based on the quantification of the total active sites of Sc_2O_3_800 and ZrO_2_HT_800 catalyst indicates that the ZrO_2_HT_800 is much more active than Sc_2O_3_800, see

Supporting Information S3. Analysis of the intrinsic reaction rate data allows assessing the specific catalytic activity of both catalysts during reaction. The 2,3-BDO conversion over Sc_2O_3_800 and ZrO_2_HT_800 catalysts at different reaction temperatures and space times is shown in Figure 12a. In the case of ZrO_2_HT_800, increasing the space time even at temperatures as low as 300°C result in approaching full 2,3-BDO conversion while increasing temperature to a minimum of 375°C is required in addition to space-time as high as 1130 kg s mol^{-1} to approach full 2,3-BDO conversion in case of Sc_2O_3_800. Thus, the specific activity of the Sc_2O_3_800 catalyst at 375°C is matched by the activity over ZrO_2_HT_800 at only 325°C, as observed in Section 4.1 and Figure 12 a. Consequently, ZrO_2_HT_800 is unequivocally a more active catalyst than Sc_2O_3_800. This superior activity is likely due to the differences in the strength, quantity, and type of active sites, suggesting distinct reaction mechanisms. From the above, we relate this to potentially an E1 mechanism being operative over ZrO_2_HT_800, resulting in the formation of MEK and *E1cb-like* mechanism over Sc_2O_3_800 for the selective formation of 3B2OL.

Furthermore, apparent activation energies of the two most important reactions, 3B2OL and MEK formation, over the two catalysts have been determined from the Arrhenius plot shown in Figure 12 b. The apparent activation energy of 3B2OL formation over Sc_2O_3_800 (63 kJ mol^{-1}) is higher than the apparent activation energy of the one over ZrO_2_HT_800 (38 kJ mol^{-1}). In contrast, the apparent activation energy of MEK formation over both catalysts are closer, i.e., 64 kJ mol^{-1} for Sc_2O_3_800 and 80 kJ mol^{-1} for ZrO_2_HT_800. These results further confirm the potential of different reaction mechanisms proposed on the basis of differences in activity, product distribution and active sites. Hence, 3B2OL formation most likely proceeds through an E2 mechanism over ZrO_2_HT_800 while it rather proceeds potentially through an *E1cb-like* mechanism over Sc_2O_3_800. MEK formation seems to follow an E1 mechanism over both catalysts. Therefore, the

activity differences discussed that originate from differences in mechanism specifically come from the stability of their corresponding intermediates, since cations are generally more stable than anions. Thus, the E1cb mechanism for Sc_2O_3_800 with anion as intermediate could be the potential reason for the higher temperature requirement to overcome its activation energy compared to E1 mechanism with cation as intermediate for ZrO_2_HT_800 catalyst which explains the fundamental differences between the performances observed on the respective catalysts.

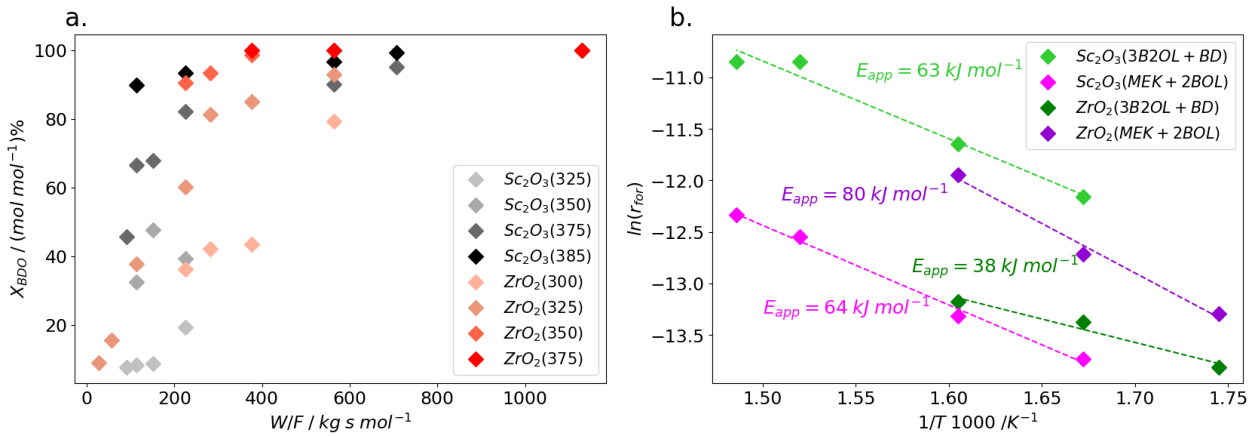

Figure 12: a. The activity of inhouse synthesized ZrO_2_HT_800 and commercial Sc_2O_3_800°C at different temperatures as a function of space-time. b. Arrhenius plot for the formation of 3B2OL and MEK over both catalysts.

The formation of MEK during 2,3-BDO dehydration can be attributed to active sites that operate according to the E1 mechanism. Despite the relatively low number of acidic sites in the Sc_2O_3_800 catalyst, as evidenced by Section 3.2, it is plausible that the formation of MEK occurs due to this acid sites. This means that an in-house preparation of the Sc_2O_3 catalyst via appropriate methods could lead to improved catalyst performance by better avoiding the presence of protonation active sites for the conversion of 2,3-BDO towards BD. In this context, comparing the findings of this work with similar other works in the literature sheds some light on whether the maximum expected performance of Sc_2O_3 as a catalyst for dehydration of 2,3-BDO towards BD has been achieved.

The product distribution obtained in the work of Duan et al. indicates a selectivity towards 3B2OL amounting to 88% (mol mol^{-1}), while the selectivity towards MEK was limited to 2% (mol mol^{-1}) [51]. In our present work, the MEK formation is almost 10 times higher than that reported by Duan [35]. This could be attributed to the difference in catalyst purity and synthesis method since the certificate of analysis indicates that trace Al and Zr are present in the catalyst used in our work. In the same work, the rate of 3B2OL formation was correlated with ionic radii of the rare earth cations Zr^{4+}, Sc^{3+} and In^{2+} being the most active for 3B2OL formation. In our present work, the catalytic performance is attributed to the acid-base functionality of the catalyst, leading to an E1cb mechanism and suggesting that the impact of ionic radii is included in the acid-base properties. A recent study demonstrates that an oxide's acidity in Smith scale using a simple linear model, decreasing ionic radii, increasing charge, increasing dipole polarizability and increasing electronegativity of metal ions result in increase in acidity of metal oxides [51,52]. From these properties, Sc_2O_3 is more acidic only in terms of electronegativity and the study confirms the base-dominated nature of Sc_2O_3 and amphoteric nature of ZrO_2.

Nakazono et al. compared various catalysts, including Sc_2O_3, either commercially acquired or in-house synthesized via different methods. Their findings indicate that hydrothermal synthesis of Sc_2O_3 followed by calcination at 800°C enhances the selective formation of 3B2OL. Furthermore, the BD-yield increased to 80% (mol mol^{-1}) at a higher temperature of 411°C. This high yield in BD could be attributed to the specific in-house synthesis methodology of pure Sc_2O_3 inhibiting the formation of MEK. The active sites proposed by the authors to be responsible for the performance as observed in their work are concerted acid-base ones similar to ZrO_2, even though the NH_3 and CO_2 poisoning experiments suggest that the basic sites are more important than acid sites which could indicate E1cb mechanism similar to the conclusion in our work.

In our present work, the catalyst characterization and thorough experimental campaign over both catalysts confirmed that the 3B2OL formation reaction over the two catalysts proceeds through different pathways, potentially, E2 and E1cb. The role of acid sites in the mechanism cannot be denied, as the occurrence of these mechanisms is not believed to represent an ‘on' or ‘off' behavior but rather exist as a spectrum of mechanisms ranging from acid-dominant mechanisms (E1) to base-dominant mechanisms (E1cb), with E2 mechanisms existing in between where both play equally important roles [48].

In summary, Sc_2O_3 exhibits great potential for BD production from 2,3-BDO dehydration. To offer an outlook from a process design perspective, different layouts should be explored since production in a single reactor may not be sufficiently selective. Instead, 3B2OL can be selectively produced in a first reactor and then more selectively converted to BD using other catalysts, as was also proposed by Zeng et al.. [38] The final choice should consider the material and energy cost of the process from an industrial perspective.

6. Conclusions

The dehydration of 2,3-butanediol (2,3-BDO) over Sc_2O_3_800 towards 1,3-butadiene (BD) was found to proceed through an *E1cb-like* mechanism catalyzed by basic sites while the remaining side products are formed via E1 reaction catalyzed by acid sites on the surface. The maximum BD yield was observed at 385°C, 1130 kg s mol^{-1}, full 2,3-BDO conversion, and an inlet 2,3-BDO partial pressure of 0.2 bar, equivalent with a selectivity towards BD of 40% (mol mol^{-1}). Sc_2O_3_800 is characterized by a constrained surface area with predominantly medium strength basic sites and even weaker and fewer acidic sites, making it a base-dominated catalyst while ZrO_2_HT_800 is more balanced in terms of number and strength of acid and base sites, suitable for an E2 mechanism.

Process conditions also exhibit a significant impact on 2,3-BDO conversion and selectivity. Temperature significantly affects 2,3-BDO conversion and consequently also the product distribution. At 325°C, the lowest 2,3-BDO conversion amounting to 8% (mol mol^{-1}) resulted in 80% (mol mol^{-1}) selectivity for 3B2OL, with MEK as the primary byproduct. At 385°C, the BD selectivity was maximal at 40% (mol mol^{-1}) with MEK accounting for 30% (mol mol^{-1}) at full 2,3-BDO conversion. Higher space times lead to the more pronounced formation of secondary products, including the desired BD, particularly at more elevated temperatures. Elevating the 2,3-BDO inlet partial pressure above 0.2 bar at higher temperatures decreases the selectivity towards 3B2OL and increases the formation of undesired secondary products. Controlling the 2,3-BDO inlet partial pressure proved to be essential to limit undesired products formation and maximize BD formation. The dehydration reaction over the Sc_2O_3_800 catalyst follows an *E1cb-like* mechanism, involving a carbanion intermediate, to produce 3B2OL. This conclusion is supported by several observations: Sc_2O_3_800 has fewer and weaker acid sites compared to its basic sites, it exhibits much lower activity than ZrO_2_HT_800, and it has a higher apparent activation energy (63 kJ mol^{-1}) compared to ZrO_2 (38 kJ mol^{-1}) for 3B2OL formation. Despite these differences, both catalysts exhibit closer activation energies for MEK formation (80 kJ mol^{-1} over ZrO_2_HT_800 and 64 kJ mol^{-1} over Sc_2O_3_800), suggesting a similar mechanism for MEK formation, potentially E2. Hence, Sc_2O_3 has a great potential for bio-based BD production either in the first step or as part of a modified catalyst for a one step double dehydration process by optimizing process conditions such as space-time, inlet partial pressure and temperature.

7. Acknowledgments

This work was performed in the framework of the Catalisti cluster SBO project SPICY ("Sugar-based chemicals and Polymers through Innovative Chemocatalysis and engineered Yeast"), with the financial support of VLAIO (Flemish Agency for Innovation and Entrepreneurship) (HBC.2017.0597).

8. References

[1] L. Du Pont, Ind. Eng. Chem. 27 (1935).

[2] A.E. Marteel-Parrish, M.A. Abraham, Green Chem. Eng. A Pathw. to Sustain. 9780470413 (2013) 1–361.

[3] J.F. Jenck, F. Agterberg, M.J. Droescher, Green Chem. 6 (2004) 544–556.

[4] G. Gwehenberger, M. Narodoslawsky, Process Saf. Environ. Prot. 86 (2008) 321–327.

[5] P. Anastas, N. Eghbali, Chem. Soc. Rev. 39 (2010) 301–312.

[6] P.C.A. Bruijnincx, B.M. Weckhuysen, Angew. Chemie - Int. Ed. 52 (2013) 11980–11987.

[7] W.C. White, Chem. Biol. Interact. 166 (2007) 10–14.

[8] F. Chang, X. Zhang, G. Zhan, Y. Duan, S. Zhang, Ind. Eng. Chem. Res. 60 (2021) 52–66.

[9] E. V. Makshina, M. Dusselier, W. Janssens, J. Degrève, P.A. Jacobs, B.F. Sels, Chem. Soc. Rev. 43 (2014) 7917–7953.

[10] D. Sun, S. Arai, H. Duan, Y. Yamada, S. Sato, Appl. Catal. A Gen. 531 (2017) 21–28.

[11] B. Török, I. Bucsi, T. Beregszászi, I. Kapocsi, Á. Molnár, J. Mol. Catal. A Chem. 107 (1996) 305–311.

[12] H. Duan, Y. Yamada, S. Sato, Chem. Lett. 45 (2016) 1036–1047.

[13] A. Igarashi, N. Ichikawa, S. Sato, R. Takahashi, T. Sodesawa, Appl. Catal. A Gen. (2006).

[14] M.C. and F.D. Guillaume Pomalaza, Paola Arango Ponton, Catal. Sci. Technol. 10 (2020)

4860–4911.

[15] K. Petrov, P. Petrova, Appl. Microbiol. Biotechnol. 84 (2009) 659–665.

[16] A.M. Ruppert, K. Weinberg, R. Palkovits, Angew. Chemie - Int. Ed. 51 (2012) 2564–2601.

[17] D. Sun, Y. Li, C. Yang, Y. Su, Y. Yamada, S. Sato, Fuel Process. Technol. 197 (2020) 106193.

[18] L.Q. Jiang, Z. Fang, F. Guo, L. Bin Yang, Bioresour. Technol. 107 (2012) 405–410.

[19] O. Hakizimana, E. Matabaro, B.H. Lee, Biotechnol. Reports 25 (2020) e00397.

[20] K. Onodera, Y. Nakaji, M. Yabushita, Y. Nakagawa, K. Tomishige, Appl. Catal. A Gen. 663 (2023) 119321.

[21] A. Matsuda, F. Sato, Y. Yamada, S. Sato, Bull. Chem. Soc. Jpn. 95 (2022) 506–512.

[22] M.A. Nikitina, V.L. Sushkevich, I.I. Ivanova, Pet. Chem. 56 (2016) 230–236.

[23] J. Zhao, D. Yu, W. Zhang, Y. Hu, T. Jiang, J. Fu, H. Huang, RSC Adv. 6 (2016) 16988–16995.

[24] W. Kim, W. Shin, K.J. Lee, Y.S. Cho, H.S. Kim, I.N. Filimonov, Appl. Catal. A Gen. 570 (2019) 148–163.

[25] F. Zeng, W.J. Tenn, S.N.V.K. Aki, J. Xu, B. Liu, K.L. Hohn, J. Catal. 344 (2016) 77–89.

[26] A. V. Tran, R.P. Chambers, Biotechnol. Bioeng. (1987).

[27] Q. Zheng, M.D. Wales, M.G. Heidlage, M. Rezac, H. Wang, S.H. Bossmann, K.L. Hohn, J. Catal. 330 (2015) 222–237.

[28] Q. Zheng, J. Xu, B. Liu, K.L. Hohn, J. Catal. 360 (2018) 221–239.

[29] H. Hattori, Stud. Surf. Sci. Catal. 78 (1993) 35–49.

[30] H. Hattori, Y. Ono, Catalysts and Catalysis for Acid-Base Reactions, Elsevier Inc., 2018.

[31] K. Stöwe, M. Armbrüster, in: Rare Earth Chem., 2020, pp. 465–485.

[32] S. Sato, R. Takahashi, M. Kobune, H. Gotoh, Appl. Catal. A Gen. 356 (2009) 57–63.

[33] A.T. Aguayo, J.M. Arandes, M. Olazar, J. Bilbao, Ind. Eng. Chem. Res. 29 (1990) 1172–1178.

[34] A. Béres, I. Hannus, I. Kiricsi, React. Kinet. Catal. Lett. 56 (1995) 55–61.

[35] H. Duan, Y. Yamada, S. Sato, Chem. Lett. 43 (2014) 1773–1775.

[36] H. Duan, Y. Yamada, S. Sato, Appl. Catal. A Gen. 491 (2015) 163–169.

[37] K. Nakazono, R. Takahashi, Y. Yamada, S. Sato, Mol. Catal. 516 (2021) 111996.

[38] F. Zeng, S.H. Bossmann, M.G. Heidlage, K.L. Hohn, Chem. Eng. Sci. 175 (2018) 387–395.

[39] B.A. Bekele, J. Poissonnier, J.W. Thybaut, J. Catal. 411 (2022) 200–211.

[40] M. Thommes, K. Kaneko, A. V. Neimark, J.P. Olivier, F. Rodriguez-Reinoso, J. Rouquerol, K.S.W. Sing, Pure Appl. Chem. 87 (2015) 1051–1069.

[41] J.M. Berty, Catal. Rev. 20 (1979) 75–96.

[42] J.W. Thybaut, C.S. Laxmi Narasimhan, J.F. Denayer, G. V. Baron, P.A. Jacobs, J.A. Martens, G.B. Marin, Ind. Eng. Chem. Res. 44 (2005) 5159–5169.

[43] J.J. Carberry, AIChE J. (1961) 350–351.

[44] C.D.P. P.B. Weisz, Adv. Catlaysis 6 (1954) 143–196.

[45] D.E. Mears, J. Catal. 20 (1971) 127–131.

[46] B. Bachiller-Baeza, I. Rodriguez-Ramos, A. Guerrero-Ruiz, Langmuir 14 (1998) 3556–3564.

[47] R.T. Morrison, R.N. Boyd, D.S. Noyce, Tetrahedron 10 (1960) 125.

[48] M.A. Aramendía, V. Borau, C. Jiménez, J.M. Marinas, A. Porras, F.J. Urbano, J. Catal. 161 (1996) 829–838.

[49] Bill Brown, (2014).

[50] R.C. Sang, Yong Pyun and Bong, Bull. Korean Chem. Soc. 26 (2005).

[51] M. Misono, in: M.B.T.-S. in S.S. and C. Misono (Ed.), Heterog. Catal. Mix. Oxides, Elsevier, 2013, pp. 25–65.

[52] W. Xing, Yngve Larring, K. Bao, Mater. Chem. (2024).